Supraglacial debris thickness variability: Impact on ablation and relation to terrain properties.

Lindsey I. Nicholson[1], Michael McCarthy[2,3], Hamish Pritchard[2] and Ian Willis[3]

[1] Department of Atmospheric and Cryospheric Sciences, Universiät Innsbruck, Innsbruck, Austria.

[2] British Antarctic Survey, United Kingdom Research and Innovation, Madingley Road, Cambridge, UK

[3] Scott Polar Research Institute, University of Cambridge, Cambridge, UK

Correspondence: lindsey.nicholson@uibk.ac.at

ABSTRACT: *Shallow ground penetrating radar (GPR) surveys are used to characterize the small-scale spatial variability of supraglacial debris thickness on a Himalayan glacier. Debris thickness varies widely over short spatial scales. Comparison across sites and glaciers suggests that the skewness and kurtosis of the debris thickness frequency distribution decrease with increasing mean debris thickness. We hypothesise that this is related to the degree of gravitational reworking the debris cover has undergone, and the effects of progressive stagnation of the underlying ice and is therefore a proxy for the maturity of surface debris covers. In the cases tested here, using a single mean debris thickness value instead of accounting for the observed small-scale debris thickness variability underestimates modelled midsummer sub-debris ablation rates by 11-30 %. While no simple relationship is found between local debris thickness and morphometric terrain parameters, analysis of the GPR data in conjunction with high-resolution terrain models provides some insight to the processes of debris gravitational reworking. Periodic sliding failure of the debris, rather than progressive mass diffusion, appears to be the main process redistributing supraglacial debris. Slope stability modelling for samples of glacier terrain suggests that the percentage of the debris-covered glacier surface area subject to debris instability can be considerable at glacier scale, indicating that up to 22 % of the debris covered area is susceptible to developing ablation hotspots associated with patches of thinner debris.*

1. Introduction

Debris-covered glaciers are the dominant form of glaciation in the Himalaya (e.g. Kraaijenbrink et al. 2017), and are common in other tectonically active mountain ranges worldwide (Benn et al. 2003). Supraglacial debris cover alters the rate at which underlying ice melts in comparison to clean ice in a manner primarily governed by the thickness of the debris cover (e.g. Østrem, 1959; Loomis, 1970; Mattson et al., 1992; Kayastha et al. 2000; Nicholson and Benn, 2006; Reid and Brock, 2010): A thin supraglacial debris cover (< a few cm) enhances melt, while thicker debris cover reduces melt by insulating the ice beneath from surface energy receipts. Prevailing weather conditions, and local debris properties, such as albedo, lithology, texture and moisture content, also influence the amount of energy available for sub-debris ablation, and modify the exact relationship between debris thickness and ablation rate. However, the general characteristics of the so-called Østrem curve are robust, demonstrating the dominant role of debris thickness in this relationship (Fig. 1).

Both theory and observations indicate that the spatial variability of supraglacial debris thickness typically has both a systematic and a non-systematic component. Debris thickness tends to increase towards the glacier margins and terminus due to concentration by decelerating ice velocity, and increasing background meltout rate (e.g. Kirkbride, 2000). This systematic variation is evident in field measurements of debris cover thickness (e.g. Zhang et al., 2011), and in characterizations of debris thickness as a function of the surface temperature distribution observed from satellite imagery (e.g. Mihalcea et al. 2006; Mihalcea et al. 2008a; Mihalcea et al. 2008b; Foster et al. 2012; Rounce and McKinney, 2014; Schauwecker et al. 2015; Gibson et al. 2017). At local scales, debris thickness varies less systematically according to the input distribution, local meltout patterns and gravitational and meltwater reworking of the supraglacial debris. Manual excavations (e.g. Reid et al., 2012), observations of debris thickness made above exposed ice cliffs (e.g. Nicholson and Benn, 2012; Nicholson and Mertes 2017), and debris thickness surveyed by ground penetrating radar (McCarthy et al., 2017) demonstrate that debris thickness varies considerably over short horizontal distances. Thus, the thickness of debris over a sampled area of glacier surface is better expressed as a probability density function than a single value (e.g. Nicholson and Benn, 2012; Reid et al., 2012). This is important because, given the strongly non-linear relationship between ablation rate and debris thickness (Fig. 1), patches of thinner debris within a generally thicker supraglacial debris cover can be expected to contribute disproportionately to glacier ablation in a manner analogous to exposed ice faces within debris-covered glacier ablation areas (e.g. Sakai et al., 2000; Juen et al., 2014; Buri et al., 2016; Thompson et al., 2016). Indeedit has been proposed that such 'ablation hotspots', along with stagnation, are the reasons for the observed similarity in surface lowering rates of otherwise comparable clean and debris-covered ice surfaces (e.g. Kääb et al., 2012, Nuimura et al., 2012).

The limited available data shows the probability density functions or frequency distribution of debris thickness at a glacier or local scale to show varying degrees of kurtosis and typically a positive skew (e.g. Reid et al., 2012; Nicholson and Benn 2012), but the degree to which the frequency distribution deviates from normal, and the controls on the degree of kurtosis and skewness have not been well investigated. Nevertheless, some postulations can be made based upon the systematic and non-systematic variability components described above. As thick debris cover tends to form where there is little to no ice flux it follows that glaciers close to steady state will tend to be dominated by thin debris, causing the debris thickness frequency distribution to have a positive skew, while this might be expected to be less pronounced in sluggish debris-covered glacier termini, or even have a negatively skewed distribution on stagnant glacier tongues or rock glaciers, where ice flux is minimal. Glaciers with patchy debris at the surface are also more likely to have a positively skewed debris thickness distribution than continuously covered glacier surfaces due to gradual topographic inversion and lateral dispersal of debris from localised surface deposits (Anderson, 2000; Kirkbride and Deline 2013). Gently sloping smooth surfaced debris covered glaciers might be expected to experience less gravitational sliding than steeper or more chaotic glacier surfaces, and less gravitational reworking may favour relatively higher kurtosis than at sites where sliding and slope failures are common, and the frequency distribution of debris thickness can be rapidly reworked and potentially even develop multimodal distributions with many areas of thin, recently destabilized debris and also many areas of thick debris where material from slope failures has accumulated.

Sub-debris ice ablation calculations are commonly performed using the mean debris thickness over a portion of the glacier surface derived, for example, from satellite thermal imagery (e.g. Fyffe et al., 2014) yet given a skewed local debris distribution, in conjunction with the asymptotic decline in ablation rate with increasing debris thickness (Fig. 1), calculations of sub-debris ice ablation rate and meltwater production using spatially-averaged mean debris thickness may differ substantially from the actual meltwater generated from a debris layer of highly variable thickness within the same area. Reid and others (2012) offered a first consideration of this effect when they applied a distributed glacier ablation model by assigning debris thicknesses to debris covered glacier pixels by random sampling of a probability distribution based on a set of high resolution field measurements. However, as yet no modelling study has explored in detail the interplay between the local debris thickness variability and the local Østrem curve, in terms of its net effect on calculated sub-debris ablation.

Given the paucity of data on local debris thickness variability there remains acritical need to quantify not only mean supraglacial debris thickness, but also local debris thickness variability, and assess its impact on ablation rate in order to understand how debris cover is likely to impact glacier behaviour, meltwater production and contribution to local hydrological resources and global sea level rise. Given the potentially significant role of accounting for debris thickness variability on glacier-wide ablation rates, it would be advantageous to be able to characterize local debris thickness variability by means of more readily observable properties. Topographic data has been used to predict soil thickness on hilly, extraglacial terrain under the assumption of steady state conditions (e.g. Pelletier and Rasmussen, 2009). However, associated soil thickness relationships as a function of slope curvature (Heimsmath et al., 2017) are based on progressive creep processes, while reworking of supraglacial debris cover occurs mainly as a result of gravitational instabilities such as ‘topples, slides and flows’ (Moore, 2017). Nevertheless, as the debris thickness that can be supported on a slope is related to slope angle, debris texture and saturation conditions (Moore, 2017) it might still be possible to find explicit relationships between topography and debris thickness. If high-resolution topography data, which is increasingly widely available, could be used to indicate local debris thickness variability, such information would complement spatially averaged mean supraglacial debris thickness values derived by other methods (cf. Arthern et al. 2006).

2. Aim of the study

This study investigates small-scale debris thickness variability, assesses the impact of local debris thickness variability on calculated sub-debris ice ablation rates, and explores the potential for predicting local debris thickness variability from morphometric terrain parameters. First, debris thickness data from shallow ground penetrating radar surveys are used to characterize the small-scale spatial variability of debris thickness on a Himalayan glacier, examine evidence of gravitational reworking processes and compare the observed variability to previously published data. Second, the impact of the observed small-scale debris thickness variability on modelled sub-debris ablation rates is assessed. Third, a contemporaneous high resolution terrain model and optical imagery are employed to determine if the observed thickness variability can be related to more readily measured surface terrain properties. Finally, a slope stability model is calibrated with the GPR and ablation model data and used to determine the percentage area of our study sites in the debris-covered ablation zone that are subject to debris instability, and potentially the formation of ablation hotspots, in mid-ablation season (August) conditions.

3. Study site and data

The Ngozumpa glacier is a large dendritic debris-covered glacier of the Eastern Himalaya, located in the upper Dudh Kosi catchment, Khumbu Himal, Nepal (Fig. 2a). The glacier has a total area of 61 km^2 of which the lower 22 km^2 is heavily debris-covered, with hummocky surface relief in the order of 50m over distances of 100m (Fig. 2b), studded with supraglacial ponds and exposed ice cliffs (Benn et al., 2001). The NE and E branches are no longer connected dynamically to the main trunk (Thompson et al., 2016), which is fed solely by the W branch descending from the flanks of Cho Oyu (8188 m). The southernmost 6.5 km of the glacier is nearly stagnant (Quincey et al. 2009) and has a low surface slope of ~4°. The terrain of this glacier, its wasting processes and the evolution of surface lakes have been well studied through a series of previous publications (Benn et al., 2000 and 2001; Thompson et al., 2012 and 2016), as have the debris properties including limited measurements of debris thickness (Nicholson and Benn, 2012).

Debris thickness over much of the debris-covered area is in excess of 1.0 m precluding widespread manual excavation. However, in 2001 measurements of debris thicknesses exposed above ice cliffs were made by theodolite survey at ~1 and 7 km from the terminus (Nicholson and Benn, 2012). These data provided only coarse estimates of debris thickness as neither the slope angle of the debris exposure, nor the impact of the theodolite bearing angle were accounted for in the vertical offsetting used to obtain the debris thickness. In April 2016 terrestrial photogrammetry was used to create a high resolution scaled model of the local glacier surface from which debris thickness estimates were made in a manner analogous to the theodolite survey at a location ~2 km from the terminus near Gokyo village (Nicholson and Mertes, 2017). At the same time, several GPR surveys, totalling 3301 m, were undertaken in this area and a single 238 m GPR survey was done close to the glacier margin ~1 km from the glacier terminus (Fig. 2a). Meteorological data are not available from the Ngozumpa glacier surface at this site, so the ablation model was forced using meteorological data measured at the Pyramid weather station (27.95° N / 86.81°E, 5035 m a.s.l.) operated by the Ev-K2-CNR consortium (http://www.evk2cnr.org/cms/en) in the neighbouring valley. A digital terrain model generated from Pleiades tri-stereo imagery acquired in April 2016 (Rieg et al., 2018) is used to relate the measured debris thicknesses to the glacier surface terrain.

4. Methods

4.1 GPR debris thickness data collection and processing

GPR measurements were made between 31st March and 20th April 2016 broadly following the methods of McCarthy et al. (2017). Debris thickness was sampled in 36 individual radar transects, covering sloping and level terrain with coarse and fine surface material. The GPR system was a dual frequency 200/600MHz IDS RIS One, mounted on a small plastic sled and drawn along the surface. Data were collected to a Lenovo Thinkpad using the IDS K2 FastWave software. This system produces two simultaneous radargrams for each acquisition. The 200 and 600 MHz antennas have separation distances of 0.230 m and 0.096 m respectively. Data acquisition used a continuous step size, a time window of 100 ms and a digitization interval of 0.024 ns. The location of the GPR system was recorded simultaneously at 1 s intervals by a low precision GPS integrated with the IDS which assigns a GPS location and time directly to every twelfth GPR trace, and by a more accurate differential GPS (dGPS) system consisting of a Trimble XH and Tornado antenna mounted on the GPR and a local base station of a Trimble Geo7X and Zephyr antenna.

Radargrams were processed in REFLEXW (Sandmeier software) by applying the steps shown in Table 1. The reflection at the ice surface was picked manually wherever it was clearly identifiable and was not picked if it was indistinct. The appropriate signal velocity for the supraglacial debris was obtained by burying a 1.5 m long steel bar to a known depth and then passing the GPR over the buried target and picking the two-way travel time to its reflection (Fig. 3a and b). Both fine and coarse material gave similar wave speeds (0.15 and 0.16 m ns^{-1}). These were averaged to obtain a bulk value that is considered representative for all the radar lines measured and is comparable to values from the debris-covered Lirung glacier, central Nepal (McCarthy et al., 2017). Debris thickness was calculated using ice surface two-way travel times and the mean of the two wave speed measurements (0.16 m ns^{-1}), taking the geometry of the GPR system into account. Uncertainties were propagated according to McCarthy et al (2017) and range from 0.14-0.83 m, generally increasing with debris thickness. According to McCarthy et al (2017), transmitter blanking is limited to one wavelength below the surface and so minimum detectable debris thickness is roughly equal to the ratio of debris wave speed to radar frequency. In our case this would imply minimum detectable debris thickness of 0.27 m with the 600 MHz antenna and 0.80 m with the 200 MHz antenna.

During processing, the integrated GPS locations (typical accuracy of ~ 3 m) were substituted for dGPS locations (typical post-processed accuracy of < 0.05 m) by matching GPS and dGPS timestamps. Where differential correction was not possible due to a lack of visible satellites, the integrated GPS locations were used. The locations of GPR data collected between timestamps were interpolated linearly in REFLEXW. Where the ice surface was identifiable in radargrams of both frequencies, the measurement made using the higher frequency was assigned because higher frequencies give higher precision. GPR data quality was assessed by comparing debris thicknesses calculated using picks from the two different frequencies in the same location (Fig. 3c) and by comparing debris thicknesses at transect crossover points (Fig. 3d). In both cases, points fit well to the 1:1 line. To show how debris thickness varies with topography, radargrams were topographically corrected for display purposes after the ice interface had been picked. Debris thickness data was extracted from the picked ice surface at approximately 0.02 m ground spacing for subsequent data analysis.

4.2 Ablation modelling

In the absence of suitable field measurements of sub-debris ice ablation, a model of ice ablation beneath a debris cover was applied to assess the impact of debris thickness variability on calculated ablation rates. As recent, high quality, local meteorological data are not available to force a time-evolving numerical model, typical ablation season conditions measured at the nearby Pyramid weather station were used to force a steady-state model of sub-debris ice ablation that has been previously published and evaluated against field data (Evatt et al., 2015).

Ice ablation conditions are generally restricted to the summer months in the eastern Nepalese Himalaya (Wagnon et al., 2013). For the illustrative simulations performed here, the model was forced with mean August meteorological conditions from 2003-2009 (<2% of August hourly data are missing), and assuming the ice temperature to be 0°C. This provides forcing variables of air temperature (3.27°C), incoming shortwave (208 Wm^{-2}) and longwave (314 Wm^{-2}) radiation, wind speed (1.94 ms^{-1}) and relative humidity (97%). Appropriate debris properties for dry debris in summer time on the Ngozumpa glacier were adopted from Nicholson and Benn (2012), whereby debris properties of effective thermal conductivity, dry surface albedo and porosity were taken to be 1.29 Wm^{-1} K^{-1}, 0.2 and 0.3 respectively. Ice albedo, debris thermal emissivity and the debris surface roughness length, friction velocity and exponential decay rate of wind were adopted from Evatt et al. (2015).

The model is used to generate an Østrem curve and associated surface debris temperature for the stated inputs, as a function of debris thickness. The model does not account for variability in surface energy receipts due to local topoclimate, or the effects of spatially or temporally variable debris properties other than thickness, and the chosen input properties are only approximate. However, this does not preclude its illustrative use in investigating the influence of variable debris thickness on calculated ablation rate. Ablation modelling was carried out using the same forcing data varying only the local debris thickness information determined at: (i) the Margin study site ~1km from the glacier terminus, (ii) the main Gokyo study site ~2 km from the terminus, both measured by GPR in 2016, and (iii) the Upglacier study site ~7 km from the terminus, measured by theodolite survey in 2001 (Fig. 2). Ablation rate and surface temperature calculated for the mean debris thickness is compared to that yielded by multiplying the percentage frequency distribution of debris thickness with the modelled Østrem and surface temperature curves. Ablation totals for the month of August are calculated and that derived using the mean debris thickness value is expressed as a percentage deviation of that derived using locally variable debris thickness. Used in this form we assume the model itself to be error free. To isolate the error associated with debris thickness, all other model inputs are also assumed to be error free. Each GPR debris thickness has an associated error, but as no quantified error assessment is available for the thickness values measured by theodolite at 7 km from the terminus a fixed error of ± 0.15 m was applied to these data. The model was run with maximum and minimum debris thickness values according to the assigned errors, to provide an indication of uncertainty of the reported percentage difference in monthly total ablation.

4.3 Terrain analysis

In order to assess the static relationship between the debris distribution and terrain properties, we used a 5 m resolution digital terrain model (DTM) derived from Pléiades optical tri-stereo imagery taken during the field campaign on the 12th April 2016. The DTM was generated from photogrammetric point clouds extracted from the Pléiades imagery, using a semi-global matching (SGM) algorithm (Hirschmüller, 2008) within the IMAGINE photogrammetry suite of ERDAS IMAGINE. The three images of each triplet were imported and the rational polynomial coefficients (RPC) provided with the Pléiades data were used to define the initial functions for transforming the sensor geometry to image geometry. With those transformation functions, individual geometries of each image in the triplet were orientated relative to each other. To obtain the most accurate exterior orientation possible, initial RPC functions were refined using automatically-extracted tie points. The calculated point clouds were then filtered for outliers, mainly found in very steep and shaded areas, using local topographic 3D filters applied in SAGA GIS software, and converted into a 5 m-resolution DTM using the average elevation of all points within one raster cell as the elevation value for the cell. Gaps were present in very steep areas, where there was cloud, and in areas with low contrast because of fresh snow or liquid water.

Terrain properties were extracted using the ArcGIS tools Slope, Aspect and Curvature. GPR data were resampled to the same resolution as these rasters (5 m) by taking the mean of the measurements that occurred within each pixel. This was done using the Point to Raster tool in ArcGIS. GPR data within 5 m of ice cliffs were excluded for comparisons made between debris thickness and topography, in order that their slope, aspect and curvature were not misrepresented. Similarly, GPR data for which dGPS locations were not available were excluded due to their lack of positional accuracy.

Ponded water at the surface is associated with the deposition of layers of fine sediments and rapid sedimentation by marginal slumping (Mertes et al., 2017). The recent history of ponded water on the parts of the glacier surface sampled by the radar transects was mapped using air photographs from 1984 (see Washburn, 1989 for details), and seven cloud-free optical satellite images spanning 2008-2016. The satellite images consisted of six Digital Globe images, and one CNES/Astrium image, all obtained via Google Earth, and the optical image from the 2016 Pleiades acquisition used to generate the DTM.

4.4 Slope stability modelling and classification

Slope stability modeling was carried out following Moore (2017). For the three study areas shown in Fig. 2, debris was classified as either stable or unstable. Unstable debris was further classified as being unstable due to:

1. Oversteepening, where surface slope exceeds the debris-ice interface friction coefficient,
2. Saturation excess, where the modeled water table height is greater than the debris thickness, and
3. Meltwater weakening, where the modeled water table height is less than the debris thickness, but debris pore pressures are sufficiently raised to cause instability.

Surface slope (see Section 4.3), modeled midsummer ablation rate (see Section 4.2), upstream contributing area, and mean debris thickness (see Section 4.1) were used as inputs to the model. Upstream contributing area was determined from the DTM in ArcGIS using the Flow Direction and Flow Accumulation tools. Sinks in the DTM were filled if they were less than 3 m deep, following Miles et al (2017), using the ArcGIS Sink and Fill tools. Surface water flowpaths were also determined using the Stream To Feature tool.

The model also requires input values for the debris-ice interface friction coefficient, the densities of water and wet debris, and the saturated hydraulic conductivity of the debris. A value of 0.5 was used for the debris-ice interface friction coefficient, following Barrette and Timco (2008) and Moore (2017). Values of 1000 and 2190 kg m^{-3} were used for the densities of water and wet debris, respectively, where wet debris was assumed to have a porosity of 0.3, after Conway and Rasmussen (2000), and the density of rock was assumed to be 2700 kg m^{-3} after Nicholson and Benn (2006). The saturated hydraulic conductivity of the debris, which is the parameter around which there is most uncertainty, was determined using the GPR data. Sections of the GPR transects, and subsequently their corresponding DTM pixels, were defined, by visual inspection on the basis of the debris morphology, as either stable or unstable. Sections of thin debris on steep slopes were considered to be unstable if they occurred among sections of thick debris on gentle slopes. Sections of anything not considered to be unstable were considered to be stable. Debris stability was then modeled for the same DTM pixels using a wide range of conductivity values. The conductivity value that minimized the difference between the number of pixels that were modeled and observed as being stable or unstable was considered to be optimal. Minimization was carried out using ROC analysis, following Fawcett (2006) and Herreid and Pellicciotti (2017). The resulting saturated hydraulic conductivity value of 40 m d^{-1} is well within the expected range of 10^{-7}-10^{3} m d^{-1} (Fetter, 1994), and is consistent with the debris being well-drained. In order to assess the robustness of the slope stability model, sensitivity tests were carried out for each study area, in which key variables of the slope stability model (ratio of densities of water to debris; saturated hydraulic conductivity; debris-ice interface friction coefficient; debris thickness and calculated daily melt rate) were perturbed, one at a time, by ± 10 %. The percentage of the study area classified as unstable, as well as percentage change from that study area's areal percentage instability (using the best estimate values given above), was recorded for each perturbation.

The percentage areal coverage of debris instability was calculated for each of the three study areas (Fig. 2). This was done both including and excluding ice cliffs and ponds, where ice cliffs and ponds were manually digitized from the orthophoto associated with the DTM.

The GPR data, DTM and associated orthophoto were collected in March/April 2016, while slope stability modeling was carried out using midsummer (August) ablation rates. It is likely that the debris on a given slope becomes more or less stable seasonally with changes in ablation rates. However, GPR observations of debris instability in March/April are likely to be representative of midsummer debris instability for saturated hydraulic conductivity as maximum melt is expected in midsummer. Similarly, while pond incidence and area vary seasonally on Himalayan glaciers, seasonal ponds commonly reform at the same sites (Miles et al., 2016), so manually digitized ponds and ice cliffs for March/April are assumed to be broadly representative of ponds and ice cliffs in midsummer for percentage area debris instability calculations excluding ponds and ice cliffs. Finally, model results should be treated only as a best approximation because the model assumes debris thickness and ablation rate are spatially homogeneous in each study area, which, as discussed by Moore (2017), is clearly not the case.

5. Results and discussion

5.1 GPR debris thickness and variability

The quality of the GPR data is generally high. The ice surface was clearly identifiable through the debris in the majority of the radargrams collected. This is likely because the GPR system was used in 'continuous-mode' and appropriate acquisition parameters were used. For those radargrams in which the ice surface was not easily identifiable, the debris appeared to be too thick to detect. While this means there is the possibility of a slight thin bias in the data, it is reasonable to assume the impact is minimal because penetration depths exceed the thickness of any supraglacial debris exposures observed in the field (Nicholson and Benn, 2012; Nicholson and Mertes, 2017). Debris thickness was found to be highly variable with a total range of 0.18 to 7.34 m (Fig. 4 and examples in Fig. 5). There is coherent structure to the debris thickness variation along transects (Fig. 4): In some areas, changes in debris thickness along the transect are gradual, while in a number of cases, there are abrupt changes in debris thickness along a transect associated with pinning points or topographic hollows and cavities in the underlying ice, which the debris cover fills (see Section 5.3 and Fig. 7).

Simple statistics of the debris thickness derived from the GPR samples of this study compared with debris thickness datasets available from other glaciers are given in Table 2. Mean debris thickness measured by GPR towards the glacier margin is thicker, and shows wider spread and lower skewness and kurtosis, than the GPR thickness data collected at the Gokyo study area (Table 2; Fig. 4; Fig. 5a-c). The percentage frequency histogram of GPR debris thickness from the glacier margin has a similar shape, but a positive offset compared to data obtained by surveying of ice faces about 1 km from the glacier terminus in 2001, while the GPR data from Gokyo agrees closely with the estimates of debris thickness from the photographic terrain model (Nicholson and Mertes, 2017). The 2001 surveyed debris thickness data from further upglacier (Nicholson and Benn, 2012) is thinner, more skewed, and has higher kurtosis than the sites further downglacier (Fig. 5a-c). Clearly, while debris thickness shows small-scale variability in all cases on the Ngozumpa glacier, the details of that variability differ from site to site. This pattern of change agrees with the tentative hypotheses proposed in the introduction, whereby the downglacier progression of greater debris cover maturity, increasingly stagnant ice and increasing activity of gravitational reworking on the hummocks terrain studded with ice cliffs and ponds all serve to gradually reduce the skew and kurtosis of the debris thickness distribution.

This pattern is supported by data from other glaciers (Table 2; Fig. 5). The medial moraine on Haut Glacier d'Arolla emerged during glacial recession in the second half of the 20th century (Reid et al., 2012), offering an example of a recently developed debris cover. The debris-covered part of Suldenferner developed its continuous debris cover since the beginning of the 19th century, when the glacier was mapped with debris cover below ~2500 m and only surficial medial moraine bands extending up to 2700 m (Finsterwalder and Lagally, 1913). The Nepalese glaciers are thought to have been debris-covered for longer (Rowan, 2016), although it remains unclear when their debris covers first developed.

The Lirung glacier measurements appear broadly more similar to sites further downglacier on the Ngozumpa glacier. Debris thickness at the Lirung glacier, central Nepal, which like the lower Ngozumpa glacier supports a thick debris cover overlying stagnant ice shows a bimodal distribution not replicated at the other sites, but partially seen in the Ngozumpa Margin site (Fig. 5a). At Lirung, this is suspected to be at least partly due to sampling bias, as the measurements were made to test the GPR method rather than to characterize typical debris thickness at this glacier. However, the hummocky terrain of Lirung glacier (cf. Fig. 2b), dissected with ponds and ice faces, is likely to facilitate widespread debris slope failure, which would more readily cause multimodal distributions of debris thickness. In contrast, debris thickness variability at the Alpine sites shown here is more comparable to that of the upper Ngozumpa, The less mature debris cover on Suldenferner, in the Italian Alps, is generally thinner and the terrain is less hummocky, with relief primarily associated with incision by supraglacial streams Debris thickness measured across the whole debris-covered area by excavation, and along cross- and down-glacier transects by GPR, shows a substantially thinner mean than the Himalayan cases, with greater kurtosis. The GPR lines sampled at Suldenferner crossed thick medial moraines and this sampling bias may explain the distribution being less skewed that that determined from the excavations covering the whole debris covered area. This highlights a further problem in sampling strategy for meaningful determinations of debris thickness variability at a local and glacier scale, as the locally less skewed distributions are presumably applicable only to sections of the glacier surface containing these medial moraines, while the debris covered ablation area as a whole shows a more skewed distribution of debris thickness. The debris cover on the medial moraine of Haut Glacier d'Arolla in the Swiss Alps is even thinner with yet more pronounced skewness and kurtosis This is inkeeping with its younger age and what might be expected from primary dispersal from the meltout of a localised moraine deposit.

The percentage frequency distributions shown in Fig. 5, viewed in the context of the relative 'maturity' of the debris covers sampled, are suggestive of a progressive change in skewness and kurtosis of debris thickness variability over time, as debris accumulates at the surface and undergoes progressively more gravitational reworking and/or the underlying ice tongue stagnates. Similarly, the observed progressive change in thickness and skewness/kurtosis of the debris sites downglacier on the Ngozumpa glacier would reflect the downglacier increase in maturity of the debris covered surface downglacier, as well as progressive stagnation of the underlying ice.

5.2 Ablation modelling using mean and variable debris thickness

Ablation was calculated using the different mean debris thickness and debris thickness variability measured at the three study areas on the Ngozumpa glacier (Fig. 2a; Fig. 5; Fig. 6a)

The ablation calculated for typical August conditions at the pyramid weather station using the mean debris thickness at the Margin, Gokyo and Upglacier sites was 2.2, 3.6 and 10.5 mm day^{-1} (Fig. 6c), totalling 0.07, 0.11 and 0.33 m of ice surface lowering over the month respectively. This agrees with the general expected patterns of ablation gradient reversal towards the terminus of a debris-covered glacier (e.g. Benn and Lehmkuhl, 2000; Bolch et al., 2008; Benn et al., 2017). Accounting for the percentage frequency distribution of debris thickness at the Margin, Gokyo and Upglacier sites increased the surface lowering rate to 2.5, 5.2 and 15.0 mm day^{-1}, giving monthly total surface lowering of 0.08, 0.16 and 0.46 m respectively. In these illustrative examples, using a mean debris thickness instead of the local frequency distribution of debris thickness, underestimates the ablation rate in these cases by 11-30 % over a month of representative August conditions (Fig. 6c). These values are specific to the cases presented here but can be considered indicative of the order of the effect of using mean debris thickness instead of the local variable debris thickness. Considering the maximum and minimum error bounds of the debris thickness distribution (Fig. 6a and c) expands the range of this underestimate to 10-40%. This suggests that while modelled ablation using local mean debris thickness can provide a lower bound this and other measures of central tendency tested but not shown here), are likely to be poor inputs for ablation modelling for typical debris cover. Instead, sufficient data points of debris thickness to capture the local variability are likely to give a more reliable ablation estimate from model simulations. As the melt rate in the 'thin debris' part of the Østrem curve responds more sensitively to changes in debris thickness than it does in the 'thick debris' part of the curve, the impact of accounting for local spatial variability in debris thickness varies inversely with debris thickness (Fig. 6c). This is compounded by the fact that thinner debris appears to have more skewness and kurtosis in the percentage frequency distribution of debris thickness, meaning that the offset between the calculated mean debris thickness and the typical debris thickness is likely to be greater. Coupled with the previous interpretations of how the skewness of debris thickness distribution relates to the relative maturity of the debris cover, this implies that the difference between sub-debris ablation calculated with a mean debris thickness of the thickness distribution will be greatest for recently developed or emerging debris cover.

Highly variable debris thickness can be expected to impact methods of mapping debris thickness using thermal-band satellite imagery, as our data show that the debris thickness variability within individual pixels of a thermal-band satellite image may be large. The modelled surface temperature for mean August conditions was 19.5, 19.0 and 16.6°C for the mean debris thickness at the Margin, Gokyo and Upglacier study areas respectively. Accounting for the local debris variability at the Margin site altered the calculated surface temperature by < 0.1°C, and, at the Gokyo and Upglacier sites, reduced the calculated surface temperatures by 0.5 and 1.5°C respectively (Fig. 6d). This highlights the manner in which variable debris thickness can be expected to influence the pixel values in satellite thermal imagery, whereby a mean debris thickness calculated from a pixel temperature can be expected to underestimate the true mean debris thickness.

5.3 Relationships between debris thickness and terrain properties

Visual inspection of the radargrams indicates that the thickest debris is found filling depressions in the underlying ice surface, and thinner debris is more commonly seen overlying steeper ice surfaces (Fig. 7a). On the basis that slope failure typically redistributes mass from areas of high slope angle, and that debris sliding was often experienced while collecting the GPR data, it seems likely that this is the result of high debris export rates from slopes to hollows due to frequent or recent slope failure in the form of sliding events (c.f. Lawson, 1979, Heimsath et al. 2012). On steeper slopes where the debris surface is approximately parallel to the ice surface, this appears to be a characteristic of debris covers at or near the limits of gravitational instability. Localized areas of thick debris are found below steep slope sections in the form of infilled ice-surface depressions. Modelled surface flowpaths (Fig. 7b) cross-cut the GPR transects where these depressions are located, indicating that they were likely incised by meltwater. This suggests that meltwater is transported in sub-debris supraglacial channels (c.f. Miles et al. 2017), but also that meltwater routing is a local control on debris thickness by providing topographic lows that become infilled by debris. Additionally, it seems likely that meltwater channels undercut steep slopes, thereby causing debris failure. Steep slopes on debris-covered glaciers are relatively short, so undercutting would have the combined effect of increasing slope angle and also reducing the confining force (or buttressing effect) imparted by down-slope debris cover. In some places, thick debris is contained behind pinning points of the underlying ice (Fig. 7a and b), which results in the occurrence of talus slopes (Fig. 7a), this stabilizes the debris and increases the confining force. Thick debris on convex, divergent terrain provides evidence of topographic inversion due to differential ablation (Fig. 7c).

The single glacier Margin transect shows increasing debris thickness towards the glacier margin (Fig. 4b and Fig. 7e). This is expected as a result of: (i) material delivered onto the glacier from the inner flanks of the lateral moraines as they are progressively debuttressed by glacier surface lowering; and (ii) lower surface velocities at the glacier margins, hence slower debris advection rates. The Ngozumpa glacier and others in the region typically have troughs at the boundary between the glacier and the lateral moraine, and evidence of thicker debris here reinforces the idea that these troughs are eroded by meltwater routed along the glacier margins (Benn et al., 2017).

Since 1984, the existence of supraglacial ponds within the Gokyo study area is likely to have affected two areas of radar transects: Several transects towards the north of the Gokyo study area, which may have been partially affected by lakes in 2012 and 2014, and a single transect towards the east of the Gokyo study area, which crossed clearly lacustrine surface deposits was partially affected by lakes in all the sampled years except 2014 and 2016 (Fig. 4). One of the transects towards the north of the Gokyo study area shows thick debris and some internal structures (Fig. 7e) including what may be a relict slump structure, where a package of sediment fell into the lake from its margin as the lake expanded (e.g. Mertes et al. 2016). Thick debris in former supraglacial lakes is likely due to high sedimentation rates in the ponds and by slumping at lake margins during lake expansion (Mertes et al. 2016). Modelling suggests that subaqueous sub-debris melt rates are low (Miles et al. 2016), so debris thickening caused by the melt-out of englacial debris is likely to be minimal. The radar stratigraphy over former lake beds suggests multiple near surface reflectors that can reasonably be interpreted as fine lake sediments overlying coarser supraglacial diamict, suggesting that the locally thicker sediments associated with lakes are due to deposition from sediment-rich supraglacial and englacial meltwaters flowing into a more sluggishly circulating pond.

The debris thickness sampled with GPR in this study does not show distinct relations with surface slope, aspect or curvature, that could be readily extracted from glacier surface terrain models (Fig. 8a, b, c). Binning the thickness data with respect to surface slope indicates a non-statistically significant step decrease in debris thickness above surface slope angles of around 20-23° (Fig. 8a). This may represent a transition from the low debris transport rates expected on low-gradient, stable slopes, to the high-debris transport rates expected on steep, failure-prone slopes. While slope and curvature are relatively evenly sampled by the dataset, the same is not true for aspect. While southerly and north-easterly aspects are well sampled, samples are scarce in other aspect sectors, rendering interpretation of potential aspect controls on debris thickness difficult (Fig 8e). Tentatively, our data suggests thin debris is scarcer for northwesterly aspects, than others (Fig. 8b, e). Comparing the GPR measurements with both slope and aspect simultaneously (Fig. 8e) shows what would be expected from Fig. 8a and 8b: That debris tends to be thicker on northwest facing slopes, and thinner on steeper slopes away from the north-westerly sector. During the pre-monsoon in the Himalaya, more melting is likely to occur on southeast-facing slopes than southwest-facing slopes because clouds often reduce incoming shortwave radiation in the afternoon (e.g. Kurosaki and Kimura, 2002; Bhatt and Nakamura, 2005, Shea et al., 2015). This effect is observable in global radiation data (Fig. 8d). Distributing incoming shortwave radiation on slopes of different slopes and aspects reveals the northwest sector to be the one receiving least solar radiation in midsummer conditions(Fig. 8f). As a result slopes in this sector may be expected to produce less meltwater meaning that debris water content, pore pressure remain low, maintaining higher shear strength and greater stability, allowing thicker debris to be sustained even on steep slopes (Moore, 2017). Samples from steep slopes in the south-east sector are scarce, likely due to the higher melt rates resulting from higher solar radiation receipts, serving to reduce slope angles here (Buri and Pellicotti, 2018). As a result of the absence of steep slopes in the southeast sector, minimum debris thicknesses are displaced to steeper slope angles flanking the aspect sector or highest midsummer solar radiation receipts. No significant correlations were found between surface curvature and debris thickness (Fig. 8c), but perhaps this is to expected, as the GPR samples only a snapshot of a dynamically evolving surface. Depending on the stage of topographic inversion sampled, thicker debris could be found at the hummock summit or in the surrounding troughs. Furthermore, the predominance of slope failure over slope creep mechanisms of gravitational reworking would serve to mask any existing relationship with curvature. Ultimately, it seems that the relationship between debris thickness and morphometric terrain parameters (slope, aspect and curvature) is complex.

5.4 Slope stability modelling

Slope stability modelling suggests that, under mid-August ablation conditions, the percentage of the debris-covered area interpreted as potentially unstable for the three study areas of Ngozumpa Glacier is between 13 and 34% including ponds and ice cliffs, and between 10 and 32% if ponds and ice cliffs are excluded (Fig. 9). The percentage of potentially unstable surface area increases upglacier, as debris thickness decreases and ablation rates increase (Fig. 6c).

Oversteepening was found to be the dominant cause of instability in all three study areas, meaning that the debris is most likely to be unstable where surface slope is greater than ~27° (i.e. greater than the inverse tangent of the debris-ice interface friction coefficient). Saturation excess was found to be the second most important cause of instability and meltwater weakening the third.

On the basis that thin debris is more likely to exist on unstable slopes, or on slopes that have recently failed, and that debris-covered glaciers typically extend to lower elevations than debris-free glaciers, these results have important implications for debris-covered glacier surface mass balance. Debris gravitational instability provides a mechanism by which relatively large parts of debris-covered glaciers can experience reworking that exposes the underlying glacier ice to high melt rates, even if the debris cover is generally thick.

Perturbing slope stability model input variables by 10% generally resulted in small changes of up to 1% in areal percentage slope instability, indicating the model is relatively robust. However, adjusting the debris-ice friction coefficient by 10% caused relatively large changes of up to 9%. Increasing melt rate and the density of water to the density of wet debris ratio cause areal percentage slope instability to increase. Increasing hydraulic conductivity, the debris-ice friction coefficient, and debris thickness cause areal percentage slope instability to decrease. It is interesting to note that the Upglacier study area is most sensitive to input variable perturbation, presumably because debris is thinner and therefore melt rate are greatest in the Upglacier study area.

6. Conclusions

Debris thickness is known to vary over the surfaces of debris-covered glaciers due to advection, rockfall from valley sides, movement by meltwater, and slow cycles of topographic inversion. The debris thickness data presented here suggest that the local debris thickness variability may show characteristic changes in skewness and kurtosis associated with progressive thickening and/or reworking of debris cover over time. On this basis the likely distribution of debris thickness might be predicted by the maturity, or time elapsed since development, of the debris cover found on a glacier surface.

For the thickly debris-covered glaciers of the Himalaya, sub-debris melt rates across the ablation zones are generally considered to be small compared to sub-aerial melt rates at ice cliffs (e.g. up to 5 cm d^{-1}, Watson et al. 2016) and sub-aqueous bare ice melt rates at supraglacial lakes (e.g. 2-4 cm d^{-1}, Miles et al. 2016). Our GPR data confirm that the debris cover on Ngozumpa Glacier is typically thick, with the thickest debris found on gentle slopes, in depressions, or at the sites of former supraglacial ponds. Here, the debris is too thick for the daily temperature wave to penetrate to the ice (Nicholson and Benn, 2012). Consequently, even in core ablation season conditions, typical melt rates are low across most of the debris covered area. However, processes of debris destabilization can form areas of thin debris within the generally thicker debris cover. These areas of thinner debris skew the spatially-averaged ablation rate in a manner that is analogous to that caused by exposed ice faces. Here, sub-debris melt rates under thinner debris are expected to be significantly above average, and even comparable with bare ice melt rates further upglacier. We find that using mean debris thickness values in surface mass balance models is likely to cause melt to be underestimated, and our results confirm previous suggestions that debris thickness is better represented in surface mass balance models as a probability density function (e.g. Nicholson and Benn, 2012; Reid et al., 2012).

On the surface of the Ngozumpa glacier, our data suggest that topography is an important additional local control on debris thickness distribution, via slope and hydrological processes, and also that thick sediment deposits at the beds of former supraglacial ponds a are an important additional control on the local variability of debris thickness. Surface debris appears to be mobilized and transported by slope- and aspect-dependent sliding caused by sub-debris melting, and most likely triggered by meltwater activity. Debris is redistributed from steep to more gentle slopes and to ice-surface depressions that are often of hydrological origin. However, the relationship between debris thickness and morphometric terrain parameters is complex. While there is some apparent variation of debris thickness with slope and aspect, whereby thinner debris caused by slope failure is more likely to occur on steeper slopes with aspects that receive more abundant solar radiation, we find no meaningful variation with curvature. This, combined with observations of slide-type debris morphology, suggests that mass movement on the Ngozumpa glacier occurs on relatively short timescales and predominantly by processes that occur at the limits of gravitational stability (e.g. Moore, 2017). Slope stability modeling suggests that large areas of the glacier are potentially prone to failure, and thus, as failure forms areas of thinner debris, that melting in these areas might be important at the glacier scale.

Data availability Debris thickness data measured on Ngozumpa glacier is available on Zenodo, DOI 10.5281/zenodo.1451559.

Author contribution LN, MM and HP contributed to field data collection. LN analyzed the debris thickness distributions, performed melt modelling and led the preparation of the manuscript. MM processed the GPR data with guidance from HP and IW,, performed terrain analysis, and slope stability modelling. All authors contributed to finalizing the manuscript.

Competing interests The authors declare that they have no conflict of interest.

Acknowledgements This research is supported by the Austrian Science Fund (FWF) projects V309 and P28521 and the Austrian Space Applications Program of the Austrian Research promotion agency (FFG) project 847999. M.M. is funded by NERC DTP grant number: NE/L002507/1 and receives CASE funding from Reynolds International Ltd. HP was funded by a British Antarctic Survey collaboration grant. The field team in Nepal was U Blumthaler, M Chand, C del Gobbo, A Groos, A Lambrecht, C Mayer, H Pritchard, L Rieg and A Wirbel. C Klug generated the DEM. Debris thicknesses data on Haut Glacier d'Arolla was collected by M Carenzo, F Pelliciotti and L Peterson and provided by T Reid.

References

Arthern, R. J., Winebrenner, D. P. and Vaughan, D. G.: Antarctic snow accumulation mapped using polarization of 4.3-cm wavelength microwave emission, J. Geophys. Res. Atmos., 111(6), 1–10, doi:10.1029/2004JD005667, 2006.

Benn, D. I., Wiseman, S. and Hands, K. a.: Growth and drainage of supraglacial lakes on debrismantled Ngozumpa Glacier, Khumbu Himal, Nepal, J. Glaciol., 47(159), 626–638, doi:10.3189/172756501781831729, 2001.

Benn, D. I., Wiseman, S. and Warren, C. R.: Rapid growth of a supraglacial lake, Ngozumpa Glacier, Khumbu Himal, Nepal, in IAHS Publication, vol. 264, pp. 177–185., 2000.

Benn, D., Thompson, S., Gulley, J., Mertes, J., Luckman, A. and Nicholson, L.: Structure and evolution of the drainage system of a Himalayan debris-covered glacier, and its relationship with patterns of mass loss, Cryosphere, 11(5), 2247–2264, doi:10.5194/tc-11-2247-2017, 2017.

Benn, D.I., Kirkbride, M., Owen, L.A. and Brazier, V.: Glaciated Valley Landsystems. In: D.J.A. Evans (Ed), Glacial Landsystems. Arnold, 2003.

Bhatt, B. C. and Nakamura, K.: Characteristics of Monsoon Rainfall around the Himalayas Revealed by TRMM Precipitation Radar, Mon. Weather Rev., 133(1), 149–165, doi:10.1175/MWR-2846.1, 2005.

Bolch, T., Buchroithner, M., Pieczonka, T. and Kunert, A.: Planimetric and volumetric glacier changes in the Khumbu Himal, Nepal, since 1962 using Corona, Landsat TM and ASTER data, J. Glaciol., 54(187), 592–600, doi:10.3189/002214308786570782, 2008.

Buri, P., Pellicciotti, F., Steiner, J. F., Evan, S. and Immerzeel, W. W.: A grid-based model of backwasting of supraglacial ice cliffs on debris-covered glaciers, Ann. Glaciol., 57(71), in press, doi:10.3189/2016AoG71A059, 2016.

Buri, P. and Pellicciotti, F.: Aspect controls the survival of ice cliffs on debris-covered glaciers, Proc. Natl. Acad. Sci., in revisio(Xx), 1–23, doi:10.1073/pnas.1713892115, 2018.

del Gobbo, C.: Debris thickness investigation of Solda glacier, southern Rhaetian Alps, Italy: Methodological considerations about the use of ground penetrating radar over a debris-covered glacier. MSc Thesis, University of Innsbruck, 2017

Conway, H. and Rasmussen, L. A.: Summer temperature profiles within supraglacial debris on Khumbu Glacier, Nepal, in IAHS Publication, vol. 264, pp. 89–97, 2000.

Evatt, G. W., Abrahams, I. D., Heil, M., Mayer, C., Kingslake, J., Mitchell, S. L., Fowler, A. C. and Clark, C. D.: Glacial melt under a porous debris layer, J. Glaciol., 61(229), 825–836, doi:10.3189/2015JoG14J235, 2015.

Fawcett, T.: An introduction to ROC analysis, Pattern Recognit. Lett., 27(8), 861–874, doi:10.1016/j.patrec.2005.10.010, 2006.

Finsterwalder, S. and lagally, M.: Die Nuevermessung des Suldenferers 1906 und dessen Veränderungen in den letzten Jahrzehnten. Zeitschrift für Gletscherkunde, 13, 1-7, 1913.

Foster, L. a., Brock, B. W., Cutler, M. E. J. and Diotri, F.: A physically based method for estimating supraglacial debris thickness from thermal band remote-sensing data, J. Glaciol., 58(210), 677–691, doi:10.3189/2012JoG11J194, 2012.

Gibson, M. J., Glasser, N. F., Quincey, D. J., Mayer, C., Rowan, A. V. and Irvine-Fynn, T. D. L.: Temporal variations in supraglacial debris distribution on Baltoro Glacier, Karakoram between 2001 and 2012, Geomorphology, 295, 572–585, doi:10.1016/j.geomorph.2017.08.012, 2017.

Heimsath, A. M., Dietrichs, W. E., Nishiizuml, K. and Finkel, R. C.: The soil production function and landscape equilibrium, Nature, 388(6640), 358–361, doi:10.1038/41056, 1997.

Herreid, S. and Pellicciotti, F.: Automated detection of ice cliffs within supraglacial debris cover, Cryosph. Discuss., (October), 1–33, doi:10.5194/tc-2017-205, 2017.

Hirschmüller, H.: Stereo processing by semiglobal matching and mutual information. IEEE Transaction on Pattern Analysis and Machine Intelligence, 30 (2), 328-341, 2008.

Hock, R. and Noetzli, C.: Area melt and discharge modelling of Storglaciären, Sweden, Ann. Glaciol., 24, 211-216, doi:10.1017/S0260305500012192, 1997

Ishikawa, M., Watanabe, T. and Nakamura, N.: Genetic differences of rock glaciers and the discontinuous mountain permafrost zone in Kanchanjunga Himal, Eastern Nepal, Permafr. Periglac. Process., 12(3), 243–253, doi:10.1002/ppp.394, 2001.

Juen, M., Mayer, C., Lambrecht, A., Han, H. D. and Liu, S.: Impact of varying debris cover thickness on ablation: a case study for Koxkar Glacier in the Tien Shan, Cryosph., 8(2), 377–386, doi:10.5194/tc-8-377-2014, 2014.

Kayastha, R. B., Takeuchi, Y., Nakawo, M. and Ageta, Y.: Practical prediction of ice melting beneath various thickness of debris cover on Khumbu Glacier, Nepal, using a positive degree-day factor, in IAHS Publication, vol. 264, pp. 71–81., 2000.

Kirkbride, M. P.: Ice-marginal geomorphology and Holocene expansion of debris-covered Tasman Glacier, New Zealand, IAHS Publ., (264), 211–217, 2000.

Kraaijenbrink, P. D. A., Bierkens, M. F. P., Lutz, A. F. and Immerzeel, W. W.: Impact of a global temperature rise of 1.5 degrees Celsius on Asia's glaciers, Nature, 549(7671), 257–260, doi:10.1038/nature23878, 2017.

Kurosaki, Y. and Kimura, F.: Relationship between Topography and Daytime Cloud Activity around Tibetan Plateau., J. Meteorol. Soc. Japan, 80(6), 1339–1355, doi:10.2151/jmsj.80.1339, 2002.

Loomis, S.R.: Morphology and ablation processes on glacier ice. Proceedings of the Association of American Geographers, 12: 88-92, 1970.

Mattson, L.E., Gardner, J.S. and Young, G.J.: Ablation on debris covered glaciers: an example from the Rakhiot Glacier, Punjab, Himalaya. In: G.J. Young (Ed.), Snow and glacier hydrology. IAHS-IASH Publication 218, Wallingford, pp. 289-296, 1993

McCarthy, M., Pritchard, H. D., Willis, I. and King, E.: Ground-penetrating radar measurements of debris thickness on Lirung Glacier, Nepal, J. Glaciol., 63(239), 534–555, doi:10.1017/jog.2017.18, 2017.

Mertes, J. R., Thompson, S. S., Booth, A. D., Gulley, J. D. and Benn, D. I.: A conceptual model of supra-glacial lake formation on debris-covered glaciers based on GPR facies analysis, Earth Surf. Process. Landforms, 42(6), 903–914, doi:10.1002/esp.4068, 2017.

Mihalcea, C., Brock, B. W., Diolaiuti, G., D'Agata, C., Citterio, M., Kirkbride, M. P., Cutler, M. E. J. and Smiraglia, C.: Using ASTER satellite and ground-based surface temperature measurements to derive supraglacial debris cover and thickness patterns on Miage Glacier (Mont Blanc Massif, Italy), Cold Reg. Sci. Technol., 52(3), 341–354, 2008.

Mihalcea, C., Mayer, C. and Diolaiuti, G.: Spatial distribution of debris thickness and melting from remote-sensing and meteorological data, at debris-covered Baltoro glacier, Karakoram, Pakistan, Ann. Glaciol., 48, 49–57, 2008.

Mihalcea, C., Mayer, C., Diolaiuti, G., Lambrecht, A., Smiraglia, C. and Tartari, G.: Ice ablation and meteorological conditions on the debris-covered area of Baltoro glacier, Karakoram, Pakistan, Ann. Glaciol., 43(1894), 292–300, 2006.

Miles, E. S., Pellicciotti, F., Willis, I. C., Steiner, J. F., Buri, P. and Arnold, N. S.: Refined energy-balance modelling of a supraglacial pond, Langtang Khola, Nepal, Ann. Glaciol., 57(71), 29–40, doi:10.3189/2016AoG71A421, 2016.

Miles, K. E., Hubbard, B., Irvine-Fynn, T. D. L., Miles, E. S., Quincey, D. J. and Rowan, A. V.: Review article: The hydrology of debris-covered glaciers; state of the science and future research directions, Cryosph. Discuss., 1–48, doi:10.5194/tc-2017-210, 2017.

Montgomery, D. R. and Dietrich, W. E.: A physically based model for the topographical control on shallow landsliding, Water Resour. Res., 30(4), 1153–1171, doi:10.1029/93WR02979, 1994.

Moore, P. L.: Stability of supraglacial debris, Earth Surf. Process. Landforms, doi:10.1002/esp.4244, 2017.

Nicholson, L. I. and Benn, D. I.: Calculating ice melt beneath a debris layer using meteorological data, J. Glaciol., 52(178), 463–470, 2006.

Nicholson, L. I. and Benn, D. I.: Properties of natural supraglacial debris in relation to modelling sub-debris ice ablation, Earth Surf. Process. Landforms, 38(5), 409–501, doi:10.1002/esp.3299, 2012.

Nicholson, L. I. and Mertes, J. R.: Thickness estimation of supraglacial debris above ice cliff exposures using a high-resolution digital surface model derived from terrestrial photography, J. Glaciol., 1–10, doi:10.1017/jog.2017.68, 2017

Nuimura, T., Fujita, K., Yamaguchi, S. and Sharma, R. R.: Elevation changes of glaciers revealed by multitemporal digital elevation models calibrated by GPS survey in the Khumbu region, Nepal Himalaya, 1992–2008, J. Glaciol., 58(210), 648–656, doi:10.3189/2012JoG11J061, 2012

Østrem, G.: Ice melting under a thin layer of moraine, and the existence of ice cores in moraine ridges. Geografiska Annaler, 51(4): 228-230, 1959.

Pelletier, J. D. and Rasmussen, C.: Geomorphically based predictive mapping of soil thickness in upland watersheds, Water Resour. Res., 45(9), doi:10.1029/2008WR007319, 2009.

Quincey, D. J., Luckman, A. and Benn, D. I.: Quantification of Everest region glacier velocities between 1992 and 2002, using satellite radar interferometry and feature tracking, J. Glaciol., 55(192), 596–606, doi:10.3189/002214309789470987, 2009.

Reid, T. D. and Brock, B. W.: Assessing ice-cliff backwasting and its contribution to total ablation of debris-covered Miage glacier, Mont Blanc massif, Italy, J. Glaciol., 60(219), 3–13, doi:10.3189/2014JoG13J045, 2014.

Reid, T. D. and Brock, B. W.: An energy-balance model for debris-covered glaciers including heat conduction through the debris layer, J. Glaciol., 56(199), 903–916, 2010.

Reid, T. D., Carenzo, M., Pellicciotti, F. and Brock, B. W.: Including debris cover effects in a distributed model of glacier ablation, J. Geophys. Res., 117(D18), 1–15, doi:10.1029/2012JD017795, 2012.

Rieg L., Klug C., Nicholson L., Sailer R. : Pléiades tri-stereo data for glacier investigations – Examples from the European Alps and the Khumbu-Himal, Remote Sens., 10(10), 1563; doi: 10.3390/rs10101563, 2018

Rounce, D. R. and McKinney, D. C.: Debris thickness of glaciers in the Everest Area (Nepal Himalaya) derived from satellite imagery using a nonlinear energy balance model, Cryosph., 8(1), 1317–1329, doi:10.5194/tc-8-1317-2014, 2014.

Sakai, A., Takeuchi, N., Fujita, K. and Nakawo, M.: Role of supraglacial ponds in the ablation process of a debris-covered glacier in the Nepal Himalayas, in IAHS Publication, vol. 265, pp. 119–132, 2000.

Schauwecker, S., Rohrer, M., Huggel, C., Kulkarni, A., Ramanathan, A. L., Salzmann, N., Stoffel, M. and Brock, B. W.: Remotely sensed debris thickness mapping of Bara Shigri Glacier, Indian Himalaya, J. Glaciol., 61(228), 675–688, doi:10.3189/2015JoG14J102, 2015.

Shea, J. M., Wagnon, P., Immerzeel, W. W., Biron, R., Brun, F. and Pellicciotti, F.: A comparative high-altitude meteorological analysis from three catchments in the Nepalese Himalaya, Int. J. Water Resour. Dev., (May), 1–27, doi:10.1080/07900627.2015.1020417, 2015.

Thompson, S. S., Benn, D. I., Dennis, K. and Luckman, A.: A rapidly growing moraine-dammed glacial lake on Ngozumpa Glacier, Nepal, Geomorphology, 145–146, 1–11, doi:10.1016/j.geomorph.2011.08.015, 2012.

Thompson, S. S., Benn, D. I., Mertes, J. and Luckman, A.: Stagnation and mass loss on a Himalayan debris-covered glacier: Processes, patterns and rates, J. Glaciol., 62(233), 467–485, doi:10.1017/jog.2016.37, 2016.

Wagnon, P., Vincent, C., Arnaud, Y., Berthier, E., Vuillermoz, E., Gruber, S., Ménégoz, M., Gilbert, A., Dumont, M., Shea, J. M., Stumm, D. and Pokhrel, B. K.: Seasonal and annual mass balances of

Mera and Pokalde glaciers (Nepal Himalaya) since 2007, Cryosphere, 7(6), 1769–1786, doi:10.5194/tc-7-1769-2013, 2013.

Washburn, B.: Mapping Mount Everest, Bull. Am. Acad. Arts Sci., 42(7), 29–44, 1989.

Watson, C. S., Quincey, D. J., Carrivick, J. L. and Smith, M. W..: The dynamics of supraglacial ponds in the Everest region, central Himalaya, Glob. Planet. Change, 142, 14–27, doi:10.1016/j.gloplacha.2016.04.008, 2016.

Zhang, Y., Fujita, K., Liu, S., Liu, Q. and Nuimura, T.: Distribution of debris thickness and its effect on ice melt at Hailuogou glacier, southeastern Tibetan Plateau, using in situ surveys and ASTER imagery, J. Glaciol., 57(206), 1147–1157, doi:10.3189/002214311798843331, 2011.

Table 1: Details of processing steps applied to radargrams, in order of use from left to right, using REFLEXW software. T is the period of the transmitted signal, t is two-way travel time and f is operating frequency.

<table>
<tr><th>operating frequency (MHz)</th><th>plateau declip</th><th>DC shift</th><th>dewow (ns)</th><th>align first breaks</th><th>timezero correct (s)</th><th>back-ground removal</th><th>band-pass filter</th><th>gain</th></tr>
<tr><td>200</td><td rowspan="2">whole profile</td><td rowspan="2">whole profile</td><td>1.5T (7.5)</td><td rowspan="2">whole profile</td><td>$7.6719e^{-10}$</td><td rowspan="2">whole profile</td><td rowspan="2">0.25f, 0.5f, 1.5f, 3f</td><td rowspan="2">divergence compensation (scaling 0.1t)</td></tr>
<tr><td>600</td><td>1.5T (7.5)</td><td>$3.2022e^{-10}$</td></tr>
</table>

Table 2: Statistics of sampled debris thickness variability measured at different locations on Ngozumpa, and other, glaciers by a range of methods.

glacier	method	source	n	m	sample/m	mean	mode	skewness	kurtosis	25%	75%	min	max
Ngozumpa	GPR*	*this study (Margin)*	13983	238	58.75	3.33	2.19	0.48	1.84	2.23	4.35	1.74	5.96
Ngozumpa	theodolite	*Nicholson and Benn, 2012 (Upglacier)*	92	460	0.20	1.65	1.87	0.87	3.76	1.05	2.14	0.12	4.36
Ngozumpa	GPR*	*this study (Gokyo)*	130926	3301	39.66	1.95	1.33	1.06	3.60	0.93	2.71	0.18	7.34
Ngozumpa	SfM-MVS	*Nicholson and Mertes, 2017*	1011	980	1.00	1.82	0.75	1.33	4.13	0.73	2.46	0.02	7.62
Ngozumpa	theodolite*	*Nicholson and Benn, 2012 (Downglacier)*	143	715	0.20	0.59	0.09	1.93	8.27	0.25	0.92	0.09	3.22
Lirung	GPR points	*McCarthy and others, 2017*	6198	354	17.51	0.66	0.39	1.07	3.24	0.32	0.93	0.11	2.30
Suldenferner	GPR	*del Gobbo, 2017*	61136	1000	61.14	0.32	0.29	0.07	3.39	0.26	0.38	0.00	0.74
Suldenferner	excavation	*del Gobbo, 2017*	101	10100	0.01	0.14	0.10	2.05	7.49	0.06	0.16	0.00	0.67
Arolla	excavation	*Reid and others, 2012*‡	488	976	0.50	0.07	0.01	6.29	68.86	0.02	0.08	0.01	1.50

* data used in ablation modelling
‡ data from medial moraine only, exlcuding patchy debris sites (< 0.01m thickness)

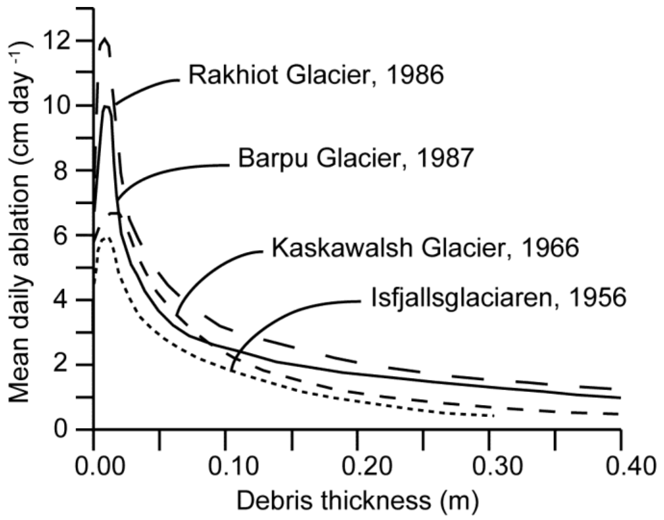

Figure 1: Examples of the relationships between supraglacial debris thickness and underlying ice ablation rate at different glacier sites, redrawn from Mattson et al. (1993). The exact form of this relationship at each site varies with prevailing meteorological conditions and debris properties, but its general character is preserved.

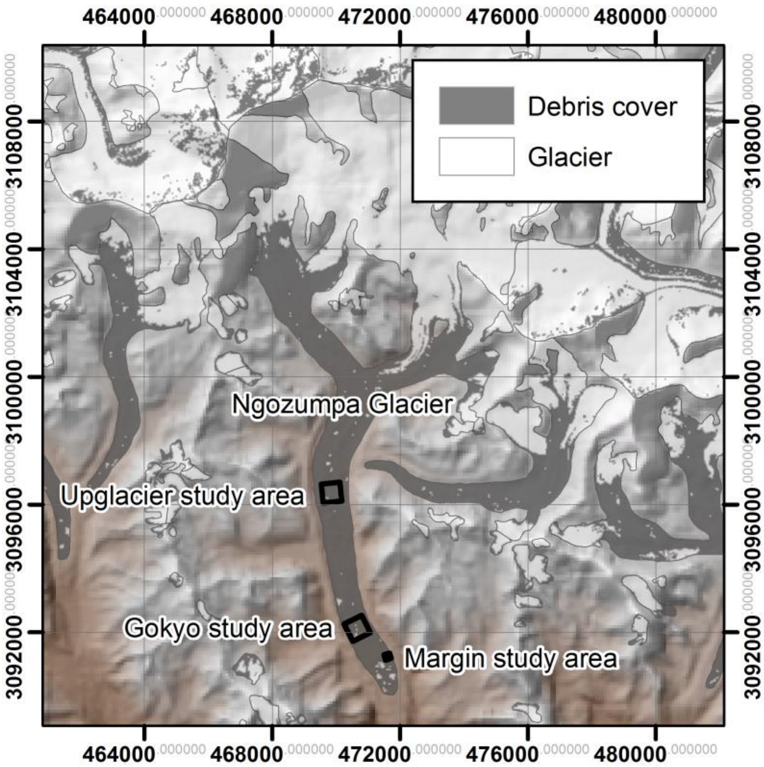

Figure 2: (a) Ngozumpa glacier showing the key study areas, ~7, 2 and 1 km from the glacier terminus at elevations of 4870, 4750 and 4740 m a.s.l. respectively (b) Photograph showing example hummocky terrain in the upglacier study area – note the people for scale in the bottom right corner. Photo credit H. Pritchard.

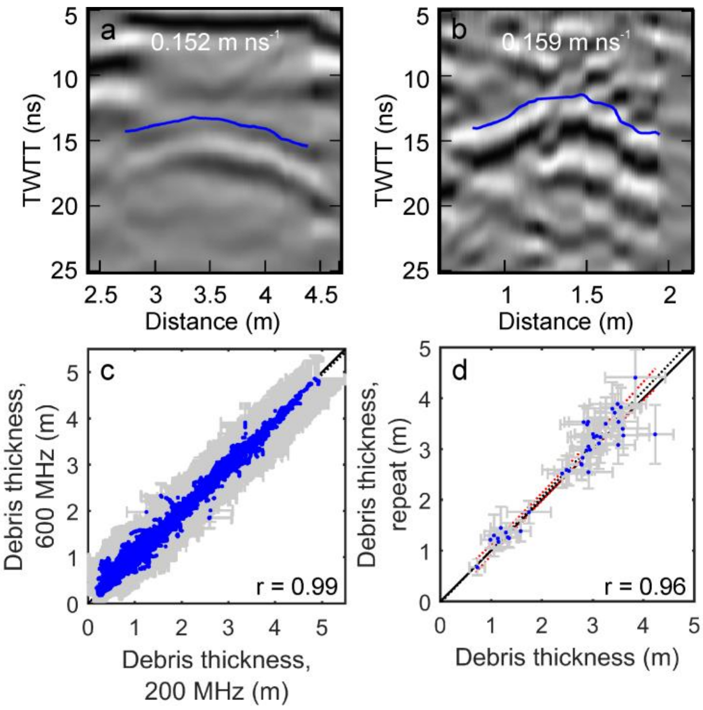

Figure 3: Reflector used to identify signal velocity on Ngozumpa glacier in (a) fine-grained sediments and (b) coarse-grained sediments. Comparison of picked debris ice interface depths sampled simultaneously with different frequencies (c) and at transect intersection points (d).

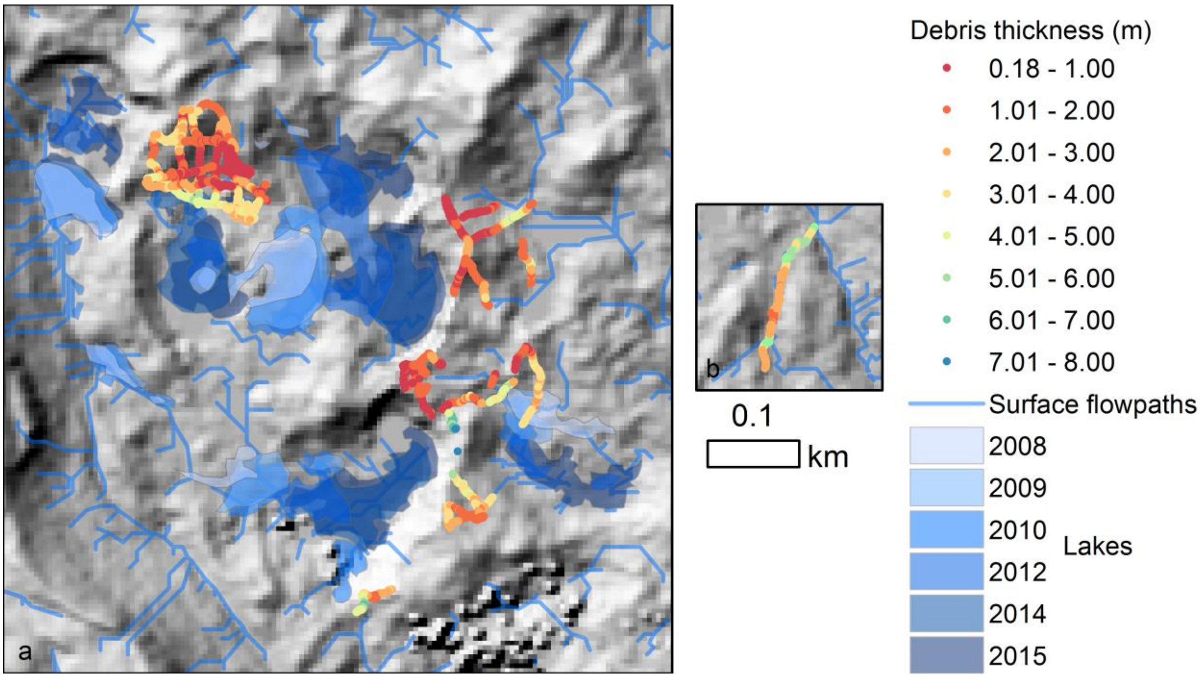

Figure 4: Overview map of GPR debris thickness sampled on Ngozumpa glacier in 2016 overlain on the hillshade from the Pleiades DTM, recent surface pond evolution, and surface flow paths for the Gokyo (a) and Margin (b) study areas (Fig. 2a).

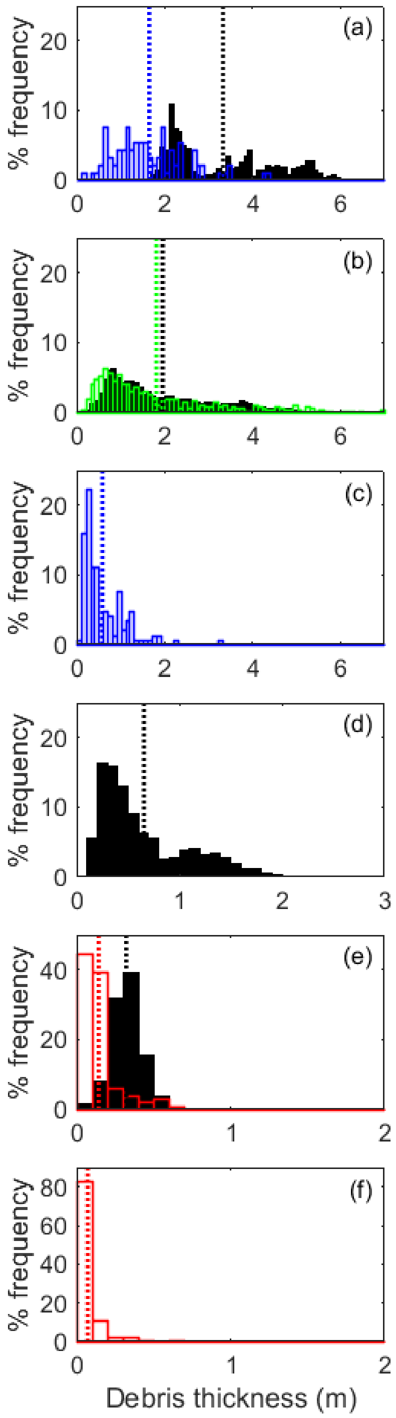

Figure 5: Percentage frequency histograms of debris thickness (h_d) in 0.1 m intervals, and mean debris thickness as vertical dashed lines for (a) the Ngozumpa Margin study site; (b) the Ngozumpa Gokyo study site;(c) the Ngozumpa Upglacier study site; (d) over the lower tongue of Lirung glacier in central Nepal; (e) across the debris covered ablation area of Suldenferner/Ghiacciaio de Solda in the Italian Alps and (f) the medial moraine of Haut Glacier d'Arolla in the Swiss Alps. Measurement methods are GPR (black); theodolite surveys (blue); Structure from Motion (SfM-MVS) photographic terrain model (green) and excavation of pits (red). Note that axes vary between sites, and summary statistics of these distributions are in Table 2.

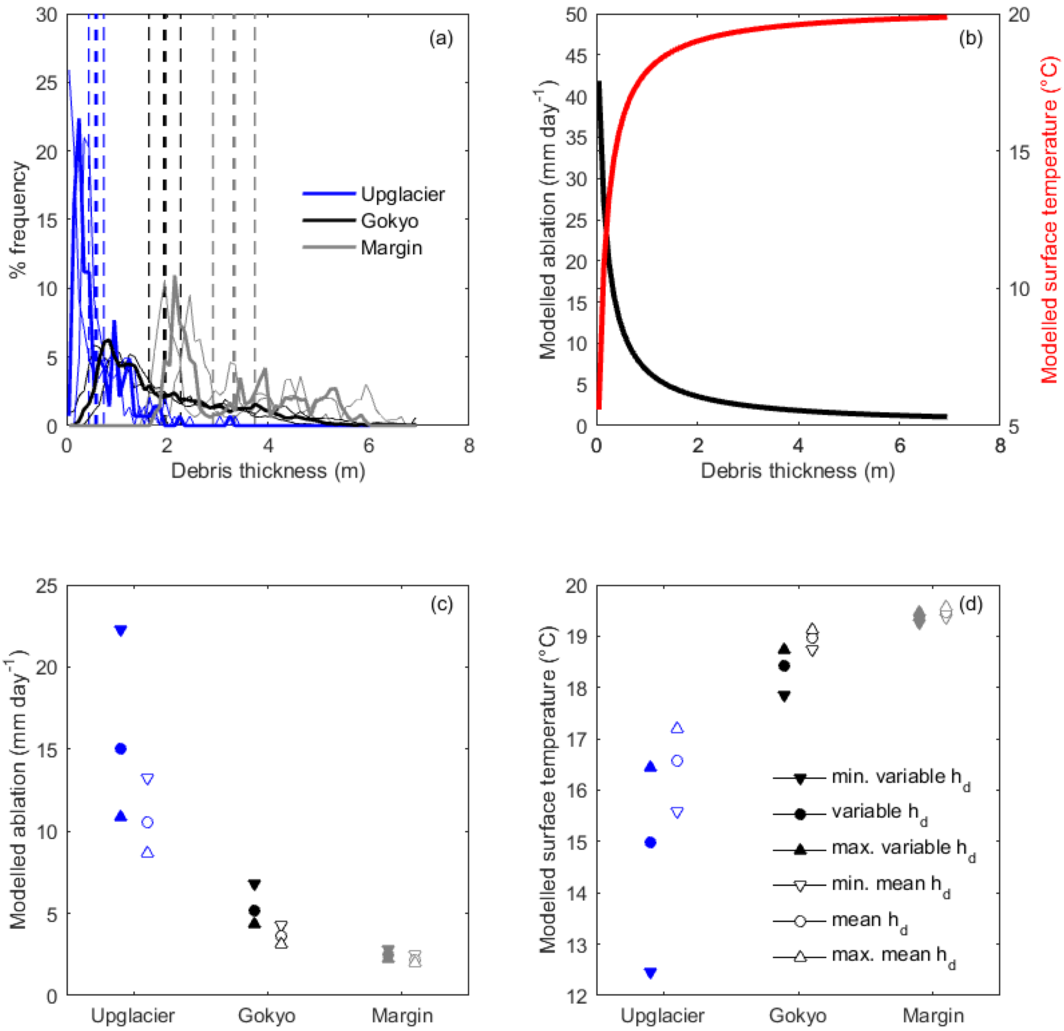

Figure 6: (a) Percentage frequency distributions from the three study sites on Ngozumpa glacier (see Fig. 1). Dashed vertical lines show the mean debris thickness at each site: 3.33, 1.95 and 0.59 m thick respectively at 1, 2 and 7 km from the terminus. Thinner lines show the values for the maximum and minimum debris thickness conditions calculated from the limits of the individual debris thickness errors. (b) Modelled Østrem curve and surface temperature for mean August conditions. (c) Comparison of modelled ablation for different representations of the debris thickness at each site. (d) Comparison of modelled surface temperature for different representations of the debris thickness at each site.

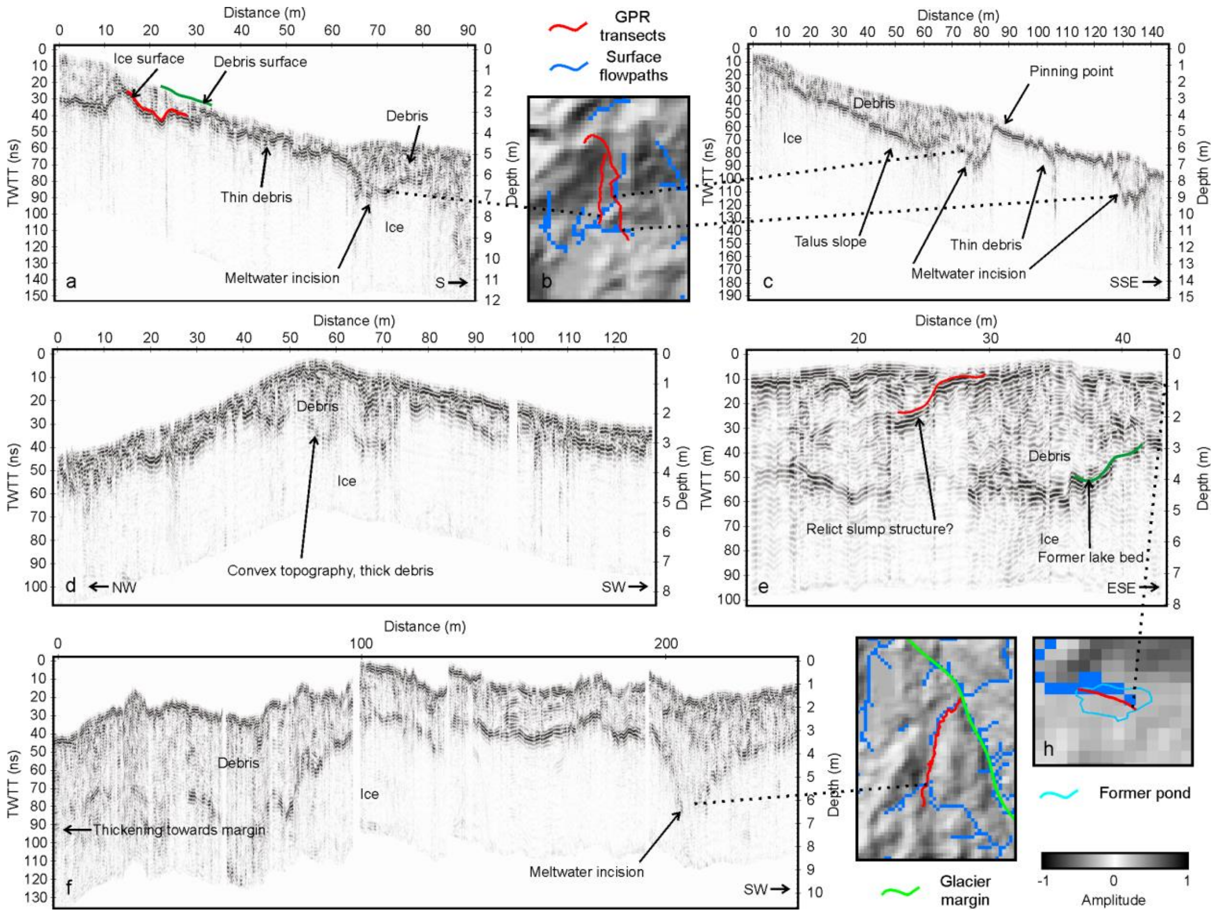

Figure 7: Example radargrams showing debris thickness variability and internal structures in relation to local topography and surface meltwater flow pathways.

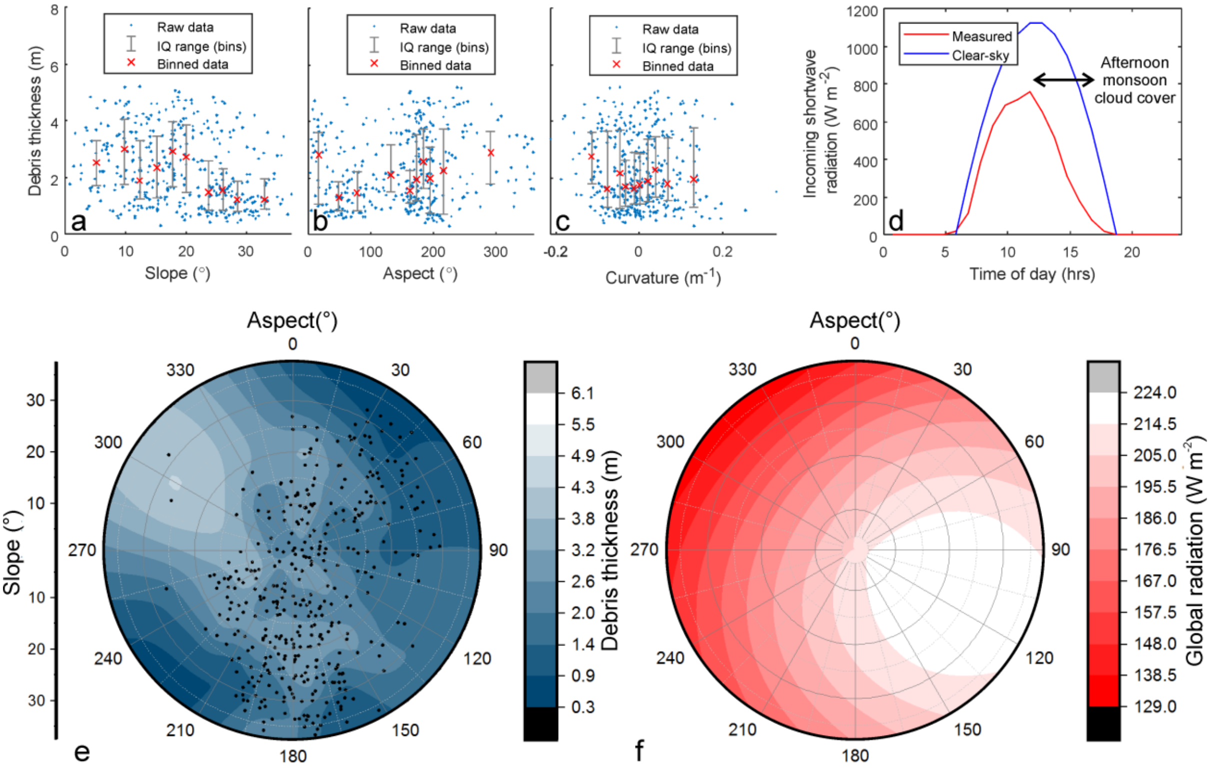

Figure 8: Summary of relationships between measured debris thickness and terrain properties: (a) debris thickness related to local slope angle; (b) debris thickness related to local slope aspect; (c) debris thickness related to curvature (d) August global radiation data collected on the glacier during the survey period; (e) hemispheric plot of debris thickness (showing sub-sampled data points) related to slope angle and aspect; (f) hemisphere plot of August global radiation, distributed on surfaces of different slope and aspect following Hock and Noezli (1997).

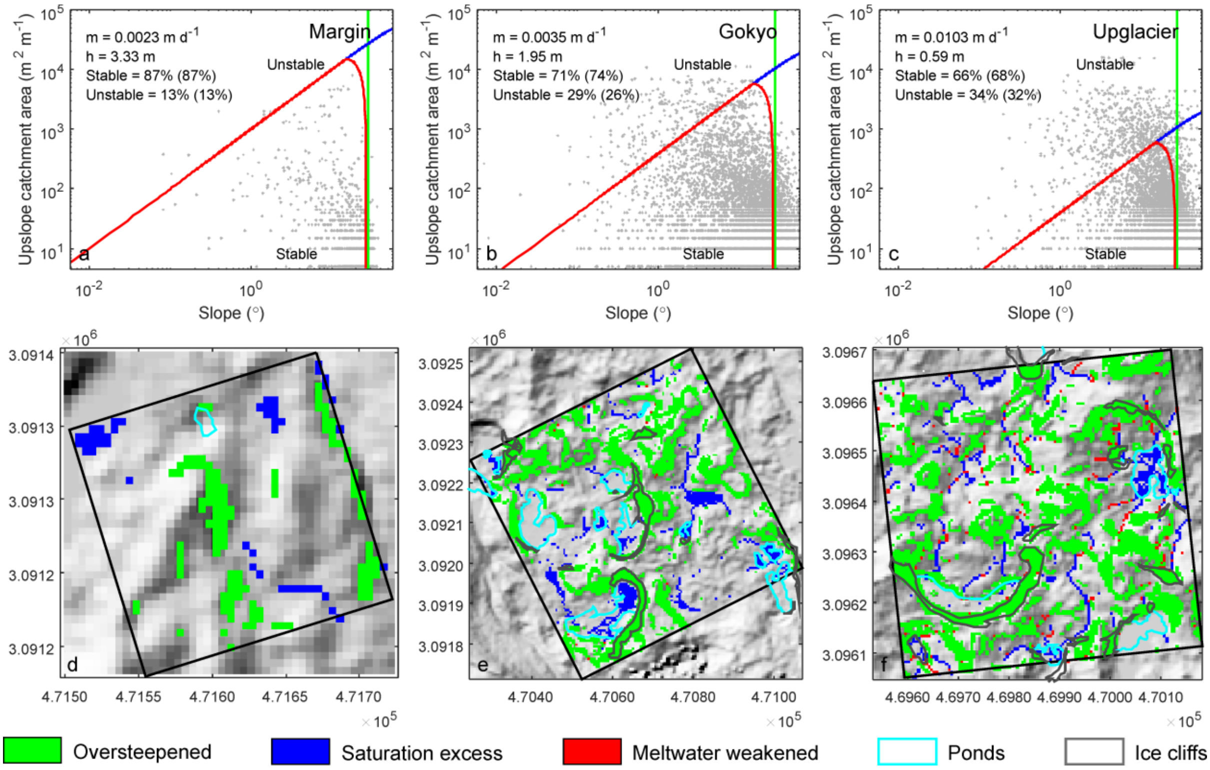

Figure 9: Results of debris stability modelling: Upslope catchment area as a function of slope angle for the three study areas (a-c); points falling above or to the right of the plotted lines are unstable. Percentage area stability/instability values are given with lakes and ice cliffs included, and in brackets with lakes and ice cliffs excluded. Maps of spatial distribution of terrain stability classifications for each study area (d-e), highlighting ponds and ice cliffs.